Short-Period Rupture Process of the 2010 M_w 8.8 Maule Earthquake in Chile

Sergio Ruiz,[a), b)] Raúl Madariaga,[a)] Maximiliano Astroza,[c)] G. Rodolfo Saragoni,[c)] María Lancieri,[d)] Christophe Vigny,[a)] and Jaime Campos[e)]

The 2010 Maule earthquake is one of the largest events ever recorded with modern instruments. We used the continuous GPS (cGPS) records to invert for the kinematic rupture process using an elliptical sub-patch approximation. In agreement with previous inversions, the largest slip is found in the northern part of the rupture zone. By cross-correlating signals from cGPS and strong motion records (SM) located in the northern part of the rupture zone, we identified two distinct seismic pulses. Using the arrival time of these pulses, we propose a short-period (<20 s) rupture process, the zone where these pulses are generated is situated near 35.5°S, in agreement with the area with the highest seismic slip and maximum observed intensity. Finally, we compare the strong motion records at the same sites for the 1985 M_w 8 Valparaíso earthquake and the Maule earthquake. We found that spectral contents and duration of the records of these two events were very similar. Thus, at least in the northern part of the rupture, the Maule earthquake radiated high frequency waves like an M_w 8 earthquake. [DOI: 10.1193/1.4000039]

INTRODUCTION

The M_w 8.8 Maule earthquake occurred in central Chile on 27 February 2010. With a rupture zone of about 500 km by 140 km, this is the largest event ever recorded instrumentally in Chile (no strong motion instruments recorded the 22 May 1960 event). The Maule earthquake has been studied by many authors (e.g., Madariaga et al. 2010, Delouis et al. 2010, Lay et al. 2010, Moreno et al. 2011, Tong et al. 2011, Lorito et al. 2011, Vigny et al. 2011, Pollitz et al. 2011, Pulido et al. 2011, among others) using a combination of low-frequency data like interferometry (few days), static GPS (>1,000 s), tsunami waveforms, and far field broad-band seismograms (>100 s). These studies provide a coherent picture of the long-period features, although these data cannot resolve whether the rupture extended all the way to the trench or was limited to the bottom part of the plate interface.

The Maule earthquake ruptured a large segment of Central Chile that covers not only the gap left by the 1835 Darwin earthquake estimated as M_w 8.3 (see Campos et al. 2002), but also the rupture zones of at least two large events of last century: the 1928 Talca earthquake

[a)] Département des Géosciences, Ecole Normale Superieure, 24 rue Lhomond, 75231 Paris cedex05, France.
[b)] Department of Geology, Universidad de Chile, Plaza Ercilla 803, Santiago, Chile.
[c)] Department of Civil Engineering, Universidad de Chile, Blanco Encalada 2002, Santiago, Chile.
[d)] Institut de Radioprotection et de Sûreté Nucléaire, Chatillon, France.
[e)] Department of Geophysics, Universidad de Chile, Blanco Encalada 2002, Santiago, Chile.

of M_w 7.7 and the 21 May 1960 Concepción earthquake of M_w 8.2. Although we lack data constraining the southern end of the rupture zone, the Maule earthquake definitely ruptured the source area of the Arauco 1975 earthquake of M_w 7.8 and may have partly ruptured the rupture zone of the Valdivia earthquake of 22 May 1960 of M_w 9.5. In the north, rupture stopped near the southern end of the Valparaíso earthquakes of 3 March 1985, M_w 8.0, and the Valparaíso earthquake of 17 August 1906, M_w 8.5. These events are depicted in Figure 1, where the rupture zones are those proposed by Campos et al. (2002). Magnitudes of the twentieth-century events are those proposed by Engdahl and Villaseñor (2002).

In spite of the large magnitude of the Maule earthquake, its maximum seismic intensity of IX was observed on low-rise rigid buildings of the city of Constitución (Astroza et al. 2012). Low intensity in rigid structures seems to be a characteristic of other large Chilean earthquakes, such as Valparaíso 1985 (EERI 1986) and Valdivia 1960 (Housner 1963). Before the 2010 Maule earthquake, the only good-quality strong motion data available in south-central Chile were those recorded during the 1985 Valparaíso earthquake (Comte et al. 1986, EERI 1986). The Valparaíso earthquake produced three main waves, or pulses, that were identified in the strong motion data by Ruiz et al. (2011). These pulses were characterized by low-displacement amplitudes, but the short-period data available for the 1985

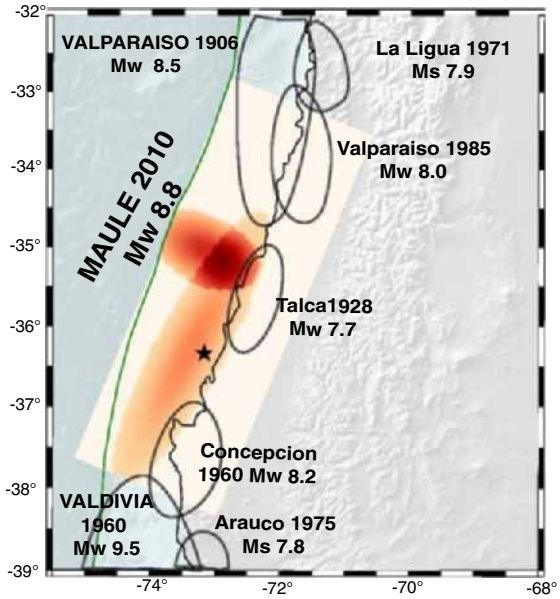

Figure 1. Rupture zone of the 2010 Maule earthquake and previous twentieth-century events of magnitudes close to 8. The star shows the low frequency epicenter of the Maule 2010 earthquake, and the orange elliptical zones are the results of intermediate frequency inversion of the Maule 2010 earthquake. Rupture zones of twentieth-century earthquakes proposed by Campos et al. (2002) are shown in black. The magnitudes of these events are from Engdahl and Villaseñor (2002). The Concepción earthquake of 21 May 1960 M_w 8.2 is a separate event from the 22 May 1960 earthquake.

earthquake did not have real-time recording, so we could not do an accurate localization of the asperities. Kiser and Ishii (2011) and Wang and Mori (2011) studied short-period waves observed in dense seismograph arrays of Japan and the United States using a back projection technique. They proposed a different high-frequency behavior of the source between regions north and south of 35.5°S. A more detailed study of short-period waves in the near field is necessary to understand the generation of high-frequency waves by the Maule earthquake. In the present paper, we invert cGPS recordings of intermediate frequency waves using a kinematic inversion method based on elliptical subsource approximation (Vallé and Bouchon 2004, DiCarli et al. 2010). Then we compare these results with the short-period waves observed in strong motion data (SM). We will use these observations in an attempt to propose a model for the origin of short-period rupture radiated by the Maule earthquake, which could be useful to understand the moderate damage observed in rigid structures like adobe and masonry houses. Interestingly, some strong motion instruments recorded both the Maule 2010 and Central Chile 1985 at the same place. We can thus compare the recordings of a megathrust event like Maule 2010 with those of a regular M_w ~8 earthquake as that of Valparaíso 1985. The comparison of these strong motion data provides information about the differences and similarities between M ~8.0 and M ~9.0 subduction events.

LONG-PERIOD AND SHORT-PERIOD HYPOCENTERS

Several different hypocenters have been proposed for the Maule 2010 earthquake by different agencies and authors, some of which are listed in Table 1. It is crucial for the successful modeling of near-field data to determine the hypocenter accurately. The main reason for the discrepancies in location is that near source data were not available for several months after the event. In the following we will use as high frequency hypocenter the location determined by the National Seismological Service of University of Chile (SSN) since they used all the short-period seismological stations that recorded the earthquake in Chile. Independently, Vigny et al. (2011) relocated the earthquake using arrival times at the high-rate GPS sites located near the earthquake. The relocated epicenter is situated about 10 km southeast of that of SSN in a region where several foreshocks occurred in December 2009 and January 2010 (Madariaga et al. 2010). In our study we will use the low frequency hypocenter of Vigny et al. (2011) to invert cGPS data and the SSN hypocenter for the modeling the short-period seismic waves. We did not use the hypocenters proposed by USGS because of the possible bias introduced by the use of far field stations situated mostly to the northeast of the hypocenter.

Table 1. Different epicenters proposed for the Maule 2010 earthquake

Latitude	Longitude	Depth	Ref
−36.25	−72.96	47.4	SSN (early determination)
−36.29	−73.24	30.1	SSN (last determination)
−35.83	−72.66	35	USGS (early determination)
−36.12	−72.90	22.9	USGS (last determination)
−36.41	−73.18	26.0	Vigny et al. (2011)

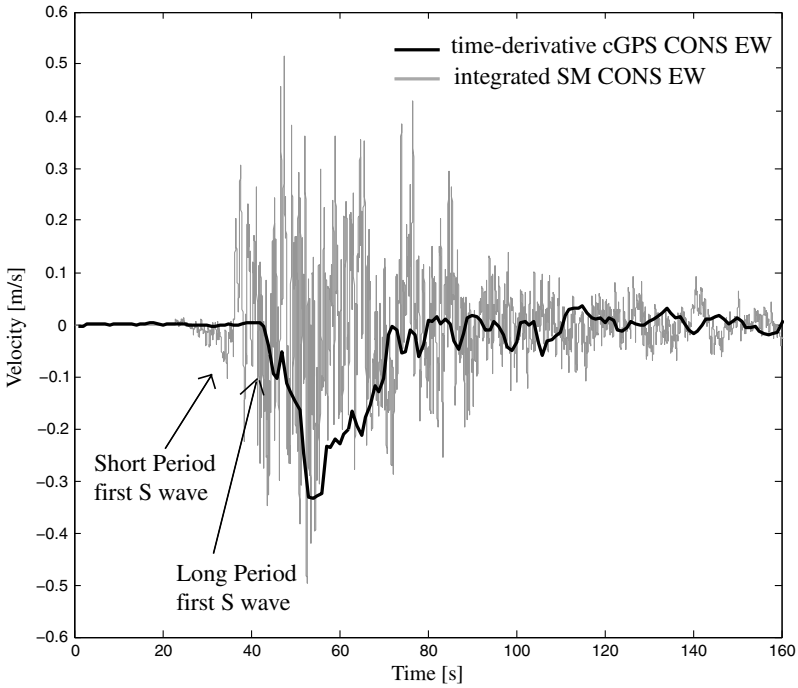

Figure 2. Ground velocity record at station CONS (Constitución) obtained from the time-derivative of the high-rate GPS record shown in black compared to the ground velocity integrated from the strong motion record at CONS. We observe a clear difference of 8–10 seconds between the high and low frequency first S wave arrivals. The cGPS time was corrected by UT + 14 leap seconds.

Figure 2 shows an example of S waves recorded in Constitución by the CONS high-rate GPS receiver and the CONS strong motion instrument. Since the strong motion instrument did not record the real time, we cross-correlated the records and shifted the strong motion. The S waves in the strong motion record appear 8–10 s before the large S wave in the high-rate GPS record. There is thus a clear difference between the high- and low-frequency origin of the seismic was. This is also apparent in the inversions by DeLouis et al. (2010).

KINEMATIC INVERSION USING HIGH RATE CGPS DATA

The Maule 2010 earthquake was the first earthquake recorded at short epicentral distances by high-rate GPS instruments at 1 Hz sampling rate (Vigny et al. 2011; see Table 2). A band passed-version of the ground displacement records obtained for the central Chile cGPS stations were used by Delouis et al. (2010) in a first inversion of the Maule event. Vigny et al. (2011) modeled the displacement records for stations in central Chile and western Argentina using the slip distribution that they determined from static GPS and inSAR interferometric data. They found excellent fit to the observed records, but high-rate GPS records were dominated by near-field static displacements so that they could not be used to determine higher-frequency details of the rupture process. In order to get intermediate

Table 2. Location of high-rate GPS instruments

Station Name	Station Code	Long.	Lat.
CONCEPCIÓN	CONZ	−36.830	−73.050
MAULE	MAUL	−35.809	−70.821
CONSTITUCIÓN	CONS	−35.330	−72.412
SAN JAVIER	SJAV	−35.595	−71.733
ROCA STO DOMINGO	RCSD	−33.653	−71.614
EL ROBLE	ROBL	−32.976	−71.015

frequency information from the high-rate GPS records, we computed ground velocity by time derivation and filtering. In Figure 3, we show the processing of the Constitución (CONS) and Concepción (CONZ) GPS records. The original displacement record is shown on top, the raw velocity in the central panel and the filtered trace from 0.005 Hz to 0.05 Hz at the bottom. The raw ground velocity record observed at CONS is very similar to a Yoffe rupture pulse (Yoffe 1951) with a total duration of only 25 s. The peak observed near 50 s (Figure 3b) is associated with the passage of the rupture front about 35 km below the station at Constitución, and the healing at 75 s is probably due to stopping phases emitted from the sides of the crack, although we cannot exclude a self-healing rupture. In any case, the duration of slip rate is about 30 s, which is significantly shorter than the total duration of the earthquake (about 90 s). The record at CONZ also has duration of 30 s, but it does not resemble a Yoffe pulse; a possible explanation is that rupture did not propagate right below the station. It must be remarked, however, that the CONZ record has a glitch a few seconds after the arrival of strong S waves (Vigny et al. 2011). At lower frequencies (Figure 4c), the two records are very similar, although CONS is 30% larger than CONZ. Since we are interested in higher frequencies, we decided to use ground velocity records obtained by bandpass-limited time derivatives of the high-rate GPS records. The records were filtered using a bandpass Butterworth causal filter between 200 s and 20 s (0.005 Hz and 0.05 Hz) see Figure 3c.

We inverted the bandpass filtered ground velocity records using an elliptical patch approximation, because we think that this approximation is adequate for situations like that of the Maule 2010 earthquake, where the cGPS station locations are roughly 100 km apart, and the velocity structure is not known in enough detail. Elliptical patch parameterization was introduced by Vallé and Bouchon (2004) to model far-field waveforms for teleseismic events. The application of the method to near-field strong-motion kinematic inversion was discussed in additional detail by Di Carli et al. (2010). This parameterization has the advantage that it produces an image of the source made of asperity-like patches. We inverted the high rate cGPS data using two elliptical patches assuming that the slip distribution D measured from the center of the ellipse had the Gaussian distribution

$$D(x, y) = D_m e^{-\left(\frac{x^2}{a^2}+\frac{y^2}{b^2}\right)} \tag{1}$$

where D_m is the maximum amplitude in the elliptical patch of semiaxes a and b. The slip distribution is continuous, but concentrated inside the ellipse. In every patch, rupture speed was assumed to be constant, and the time of rupture t_r was computed with respect to distance

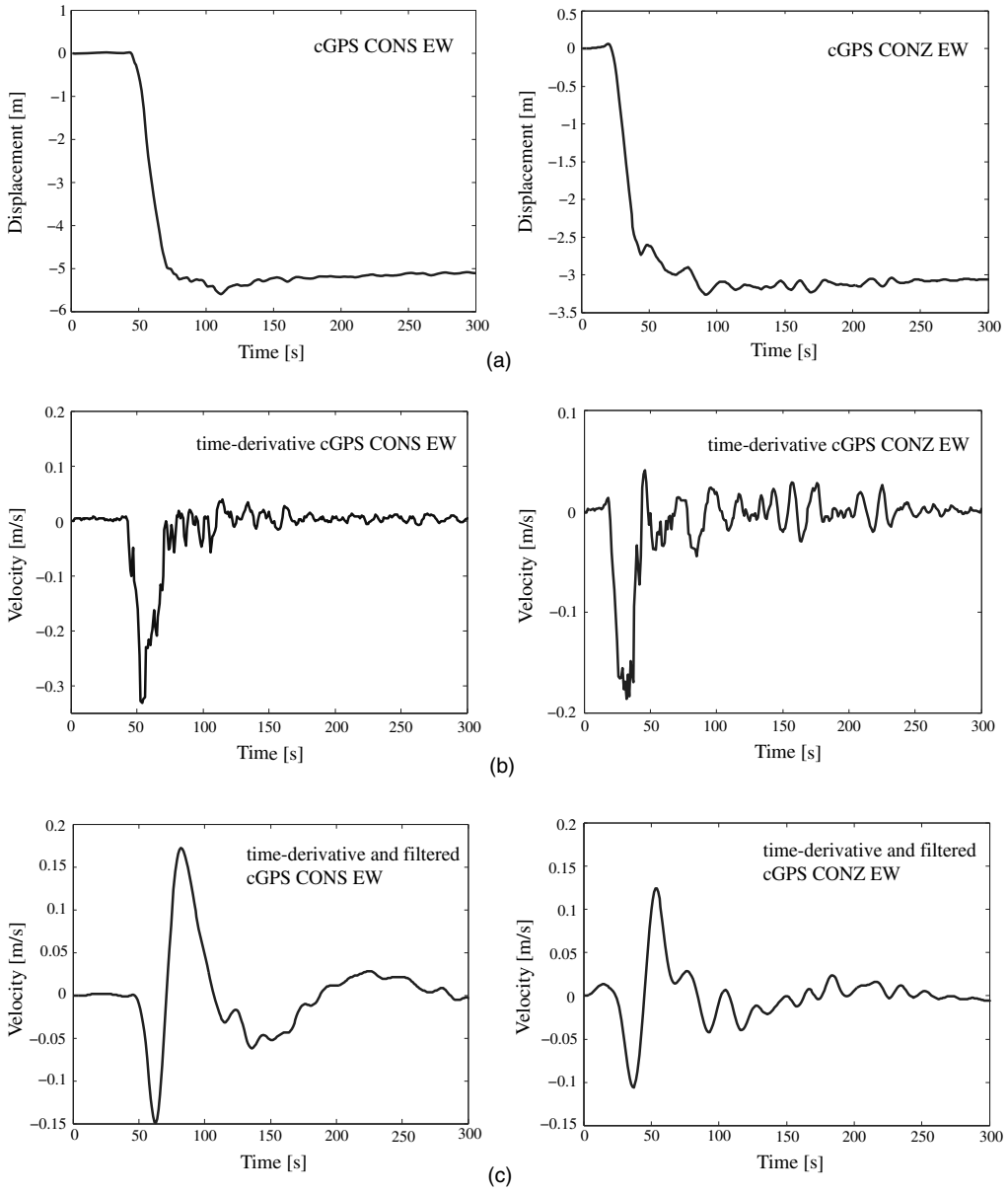

Figure 3. (a) High-rate GPS EW displacement records at CONS EW and CONZ EW, see Figure 4 and Table 3 for the location of the GPS antennas. (b) Time-derivative of the CONS and CONZ EW records. (c) Ground velocity records at CONS EW and CONZ EW filtered between 0.005 and 0.05 Hz (200 s to 20 s period).

from the hypocenter in order to insure causality in the forward models. Slip rate on every patch was also very simple. The source time function at any point on the fault was a triangular function of total duration $t = 10$ s around the rupture time t_r. This duration is shorter than that of the ground velocity records at CONZ and CONS shown in Figure 3b. In the forward model, each elliptical patch is described by seven parameters: two coordinates of the center, two semiaxes a and b, an angle of orientation α, slip amplitude D_m, and rupture speed v_r. The AXITRA code (Coutant 1990, Bouchon 1981) was used to simulate wave propagation from the source to the receivers using the velocity model of Campos et al. (2002). The fit between observed (*obs*) and synthetic (*synth*) records was measured with the L2 norm:

$$\chi^2 = \frac{\sum_i (obs_i - synth_i)^2}{\sum_i (obs_i)^2} \tag{2}$$

where the index i runs over all samples in every seismogram considered in the inversion. The neighborhood algorithm (NA) of Sambridge (1999) was chosen to search for the minimum value of the L2 norm.

Figure 4 shows the slip distribution results and the rupture time isochrones for the best solution found by the NA algorithm. This solution has a misfit $\chi^2 = 0.43$. We modeled the earthquake with two elliptical patches: the maximum slip is larger than 10 m in the northern zone, and the rupture velocity in each ellipse is close to 2.5 km/s. There is not enough resolution in our data to increase the number of ellipses. Figure 5 shows the fit between observed

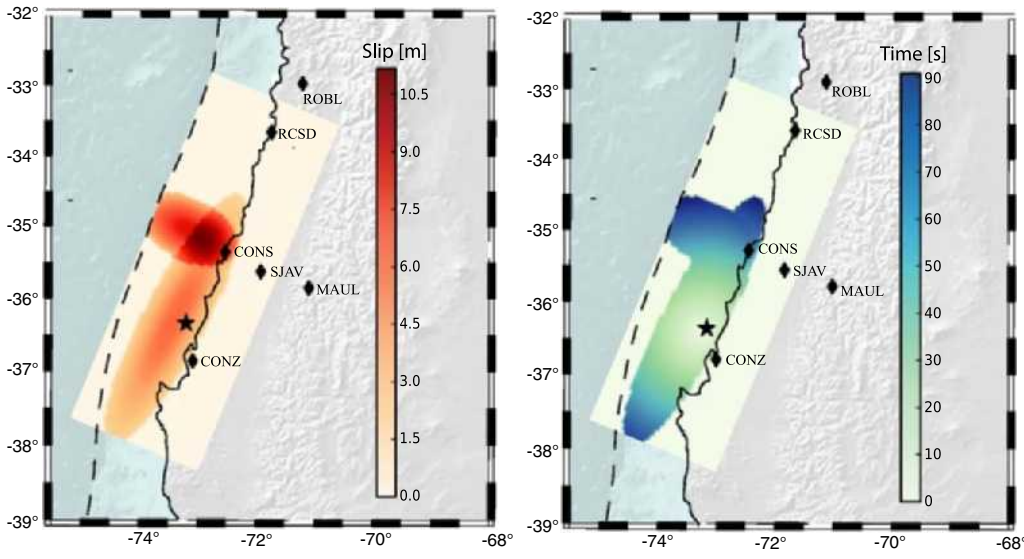

Figure 4. Result of kinematic inversion of ground velocity records time-derivative from high-rate cGPS data. On the left (a) slip distribution; and on the right (b) rupture time. Diamonds are locations of cGPS stations used in our inversions, dashed line is ocean trench (plate boundary between Nazca and South American Plates), star is the long-period epicenter.

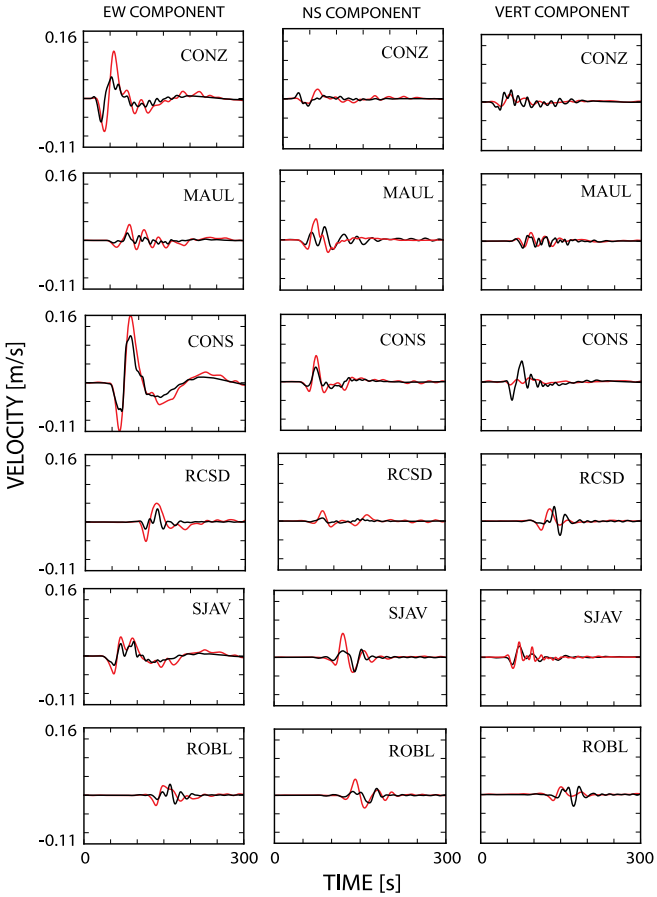

Figure 5. Comparison of observed (red) and synthetic (black) ground velocity derived from cGPS records. Both synthetic and observed records were causally filtered between 0.005 Hz and 0.05 Hz (200 s to 20 s period).

and synthetic ground velocity derived from high-rate GPS data. The initial time of observed and modeled records is the same, confirming the proposed long-period hypocenter of Vigny et al. (2011) and the position of two elliptical slip patches. On the other hand, not only the long-period waves are fitted as observed in EW CONS record, but also intermediate frequency waves as observed in the SJAV EW record. The fit could certainly be improved but the records are sparse, and we lack instruments in the southern end of the rupture zone. For this reason, we believe that the solution of Figure 4 models well only the northern part of the rupture. Unfortunately, there is no seismic data that can be used to study the southern part of the rupture process.

SHORT-PERIOD RUPTURE PROCESS OF THE 2010 MAULE EARTHQUAKE

The Maule 2010 earthquake was recorded by the high-rate GPS instruments sampled at 1 Hz that we inverted in the last section. It was also recorded by more than 30 strong motion

instruments; unfortunately, few of them recorded the absolute time, and most had a very short pre-event buffer memory (Boroschek et al. 2012). As with high-rate GPS, the northern zone of the rupture is more densely instrumented (Boroschek et al. 2012, Vigny et al. 2011). For this reason, we studied in more detail the short-period characteristics of the rupture in this zone. This region is very interesting because of the high seismic intensities recorded there when compared to the southern part of the rupture (see Astroza et al. 2012).

The strong motion data recorded in the northern part of the earthquake show two important arrivals for periods lower than 20 s (Figure 6). This figure shows the ground displacement computed from strong motion data between 34°S and 36°S. The accelerograms were filtered using a Butterworth non-causal filter between 20 s and 0.05 s (0.05 Hz and 20 Hz), the baseline was removed, and then the records were integrated twice to compute displacements. In these records, it is possible to clearly identify two main pulses. The components where the pulses were better observed are plotted in Figure 6. Since these pulses arrive at different times at the stations of the network, it was possible to identify the area on the fault where they were generated; these zones will be called "asperities," following the original idea of Kanamori and Stewart (1978). The overall duration of the records shown in Figure 6 is about 60 s, but the individual pulses observed in the different stations are on the order of 10 s to 15 s. This is significantly lower than the overall duration of the earthquake, which was about 90 s. For this reason, we propose that the pulses were emitted by localized asperities that break on top of the large-scale rupture process. From the cross-correlation of the records, we concluded that these asperities were located in the northern zone of the rupture, separated at most by a few tens of kilometers.

The asperities were identified using the displacement records shown in Figure 6. Of these records, only station Convento Viejo (CONV) had absolute time. Fortunately, as we showed

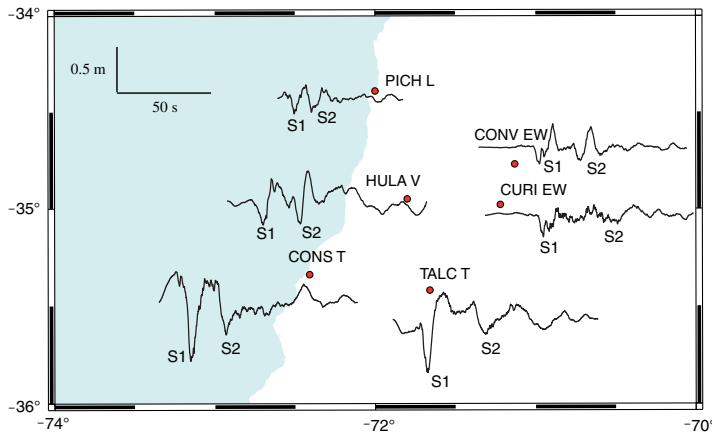

Figure 6. Strong motion displacement records located between −34° to −36°. Station locations are listed in Table 2. Not all instrument are oriented along geographical coordinate L, T, and V refer to Longitudinal, Transversal, and Vertical, that unfortunately not always have the same orientation. S1 and S2 correspond to named pulse 1 and pulse 2 inside of the text.

in Figure 2, the strong motion instrument in Constitución was located very close to the cGPS antenna CONS. Cross-correlating these two records, we could assign absolute time to the CONS strong motion record. For the other four records, the time was determined by comparing the theoretical S arrival time from the high frequency hypocenter and the observed first S arrival in the strong motion record (Figure 7a).

Figure 7 shows the normalized strong motion displacement records at the same stations shown in Figure 6. The seismic traces are located along the ordinate of the plot as a function of the distance in kilometers from the SSN epicenter or proposed asperity hypocenter (Table 3), and the abscissa is time in seconds. The curves plotted on top of the seismic section are the travel times computed using the layered velocity model derived from local data by Campos et al. (2002).

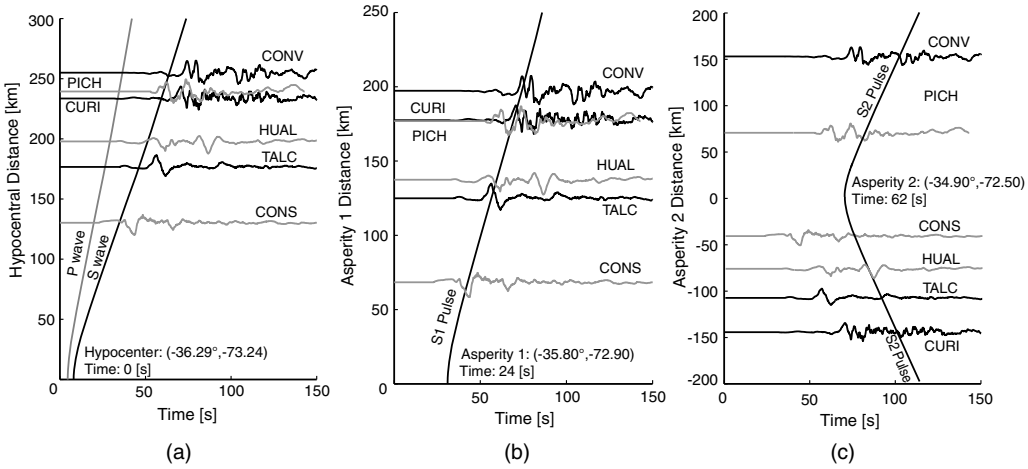

Figure 7. (a) Strong motion displacement record as a function of distance to the hypocenter. (b) and (c): Strong motion displacement record as a function of distance to asperities 1 and 2, respectively. The gray curves are the time-distance calculated for (a) P waves (gray curve) and S waves (black curve); (b) and (c) for S1 and S2 pulses. The hypocenter a location of asperities is shown. Time axis in each figure is the time of start of wave propagation from the hypocenter (a) and asperities (b and c).

Table 3. Location of the hypocenter and asperities of the Maule 2010 earthquake

	Latitude	Longitude	Depth (km)
SSN Hypocenter	−36.29	−73.24	30.1
Asperity 1	−35.80	−72.90	25
Asperity 2	−34.90	−72.50	25

We tested different locations of the asperities until we found the best fit between computed arrival times of pulses emitted by possible asperities and the observed pulses in the strong motion displacement records. The rupture velocity found from the inversion of the cGPS records (~2.5 km/s) was used. The best locations of the two asperities are shown in Table 3. The fit between the theoretical arrival of S waves from asperities and observed pulses are presented in Figures 7b and 7c. We obtained a good fit between the theoretical arrival of S waves and observed pulses; the small difference between theoretical and observed arrival time can be explained by the simplicity of the one-dimensional velocity model considered, the assumption of constant rupture velocity, or because the travel times were computed assuming that the asperities were located at a single point. Clearly, more detailed numerical modeling that takes into account a better structural model will be needed to improve this initial schematic model. However, the good fit allows us to assume that displacement pulses observed in strong ground motion are directly associated to S waves that originate from the proposed location of the asperities.

The proposed locations of the two asperities were checked using the high-rate GPS displacement records at the stations listed in Table 2; Figure 8 shows these records. The travel times computed using the layered velocity model proposed by Campos et al. (2002) do not fit

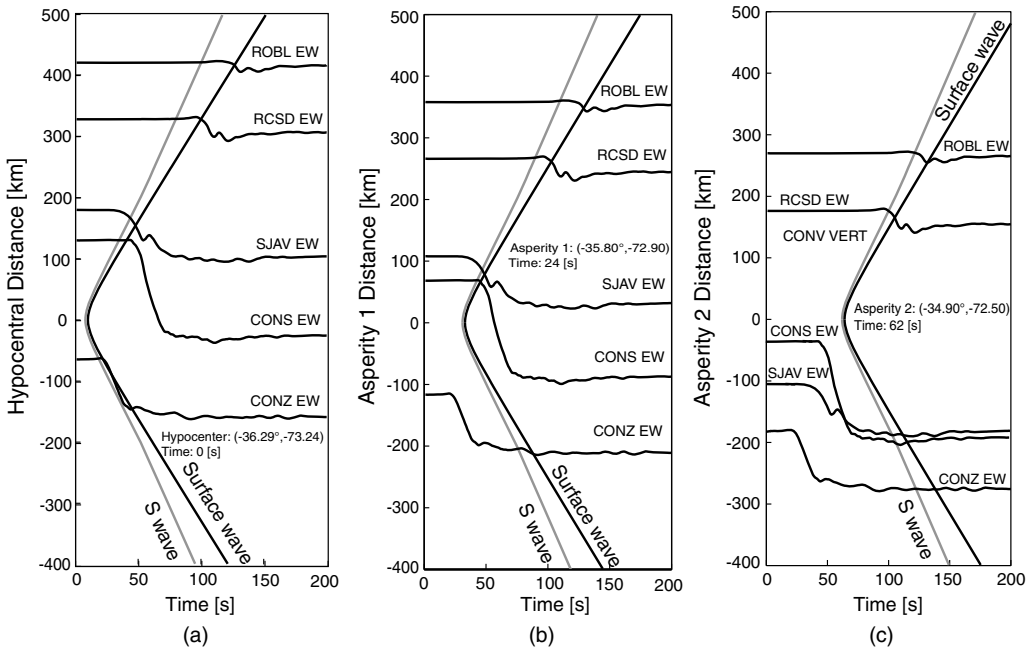

Figure 8. (a) cGPS as a function of distance to hypocenter. (b) and (c): cGPS as a function of distance to asperities 1 and 2, respectively. The gray curves are the curves time-distance calculated using Campos et al. (2002) velocity model and the black curve are the curves time-distance calculated using a crustal shear velocity. The Time in each figure is the time of start of wave propagation from the hypocenter (a) and asperities (b and c).

well with the observed arrivals of S waves from asperities in the high-rate GPS stations. For this reason, new travel-time curves were computed using a simple homogeneous crustal shear speed of 3.3 km/s; these travel times fit very well the first arrival of the S wave at the different high-rate GPS stations, as well as with the arrivals of the two observed pulses in ROBL and RCSD, which in this case are associated with surface waves that propagate in the crustal wave guide. These pulses are easily identified in the northern components of the cGPS stations, although the second pulse is difficult to identify in the SJAV record. This is probably an effect of the northward propagation of rupture, since SJAV is located south of the second asperity. Along the coast at CONZ and CONS, the pulses are very difficult to identify because they are hidden by the strong near-field displacement due to the passage of the seismic rupture.

In conclusion, the short-period rupture process is schematically shown in Figure 9 where we plot the location of the hypocenter, the asperities and the direction of rupture propagation. The short-period rupture propagates northwards from the hypocenter and has shorter duration than the overall duration of the Maule 2010 earthquake and its source area is smaller than that of the low frequency rupture of the earthquake. This short-period rupture has a rupture area and duration similar to that of an M_w ~8.0 earthquake, because the two asperities we identified in Figure 9 have sizes similar to the rupture area of a magnitude 8 event in central Chile (Ruiz et al. 2011). The zone where these strong motion short-period waves were emitted agrees with the area of higher seismic intensity (MSK > VIII) observed by Astroza et al. (2012).

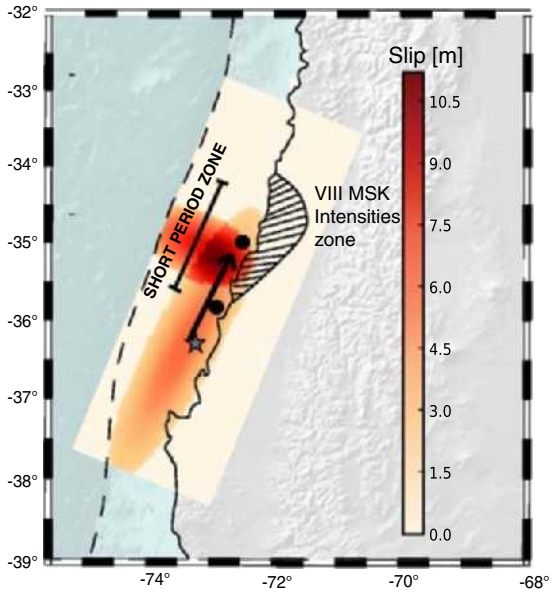

Figure 9. Representations of short-period rupture process. The rupture start from the hypocenter (star) propagating towards two asperities (black large dots) located to the north. The color zone is the rupture area of Maule 2010 earthquake. The dashed area is the zone of strong seismic intensity (MSK > VIII) of the Maule 2010 identified by Astroza et al. (2012).

COMPARISON WITH THE VALPARAÍSO 1985 STRONG MOTION RECORDS

The Valparaíso 1985 (M_w 8.0) earthquake broke a rupture zone situated immediately to the north of the Maule 2010 earthquake (see Figure 1). Fortunately, a few strong motion instruments located in central Chile recorded both events, as shown in Figures 10a and 10b. We can use these records to compare the characteristics of these two events. As observed in Figures 10a and 10b, records from the 1985 and 2010 events had similar amplitudes and durations at stations PICH, LLOL, and MELP, which are located north of the rupture zone of the Maule 2010 earthquake and in the south-central part of that of Valparaíso 1985. The PAPU, ZAPA, UTFS, and VINA stations have similar amplitude but shorter duration for the Maule records, and TALC has a shorter duration for Valparaíso 1985. The different duration of these records could be explained by the different directions of the rupture propagation of both earthquakes, south to north by the Maule 2010 and north to south for the 1985 Valparaíso earthquake (Figure 10c). Finally, in Figure 10d, the response spectra of acceleration with 5% damping are compared for the two earthquakes, showing similar spectra for both events, except for the TALC (Talca) recordings.

Similar pulses to those observed in the Maule 2010 were identified in the strong motion records of the Valparaíso 1985 earthquake and also in Tocopilla 2007 (M_w 7.7) Chile earthquake (Ruiz et al. 2011), confirming that the short-period waves generated by the Maule 2010 earthquake are similar to those observed in M_w ~8.0 Chilean subduction earthquakes.

DISCUSSION

The Maule megathrust earthquake was a very large event (M_w 8.8) in the long-period domain (>100 s), with far-field ground motion dominated by the overall rupture process. We recomputed the slip distribution, using band-limited ground velocities derived from high-rate GPS records. The slip distribution we propose (see Figure 4) is very similar to results proposed by others authors in terms of the spatial pattern, especially for the locations of largest slip in the northern part of the rupture zone (e.g., Delouis et al. 2011, Vigny et al. 2011, etc.). However, at short periods, a different picture emerges, where radiation, as observed in strong motion records, appears to be mostly controlled by two asperities. These asperities produced pulses of similar duration and amplitude as those observed in previous Chilean subduction earthquakes with M_w close to 8.0. The short-period rupture process of this megathrust earthquake may explain why some strong motion records of the Valparaíso earthquake of 1985 are similar to those of the Maule 2010 earthquake. Although the southern part of the Maule earthquake rupture is not well instrumented, our rupture process agrees with the back propagation results of Kiser and Ishii (2011) and Wang and Mori (2011). These authors found that more short-period energy was emitted in the northern zone of the rupture compared to the southern one. Both groups detected an important velocity change in the rupture propagation around 35.5°S. It is important to emphasize here that these authors located the strong sources of high frequencies with respect to the USGS hypocenter. This may produce an artificial shift of their source to the east and perhaps to the north because the USGS hypocenter does not agree with either short or long-period near-field data. The location of the low-frequency hypocenter (Vigny et al. 2011) further to the west and south, with respect to the USGS hypocenter, is required by the arrival times of long-period waves at high-rate GPS records in central Chile. The actual location of the hypocenter may have

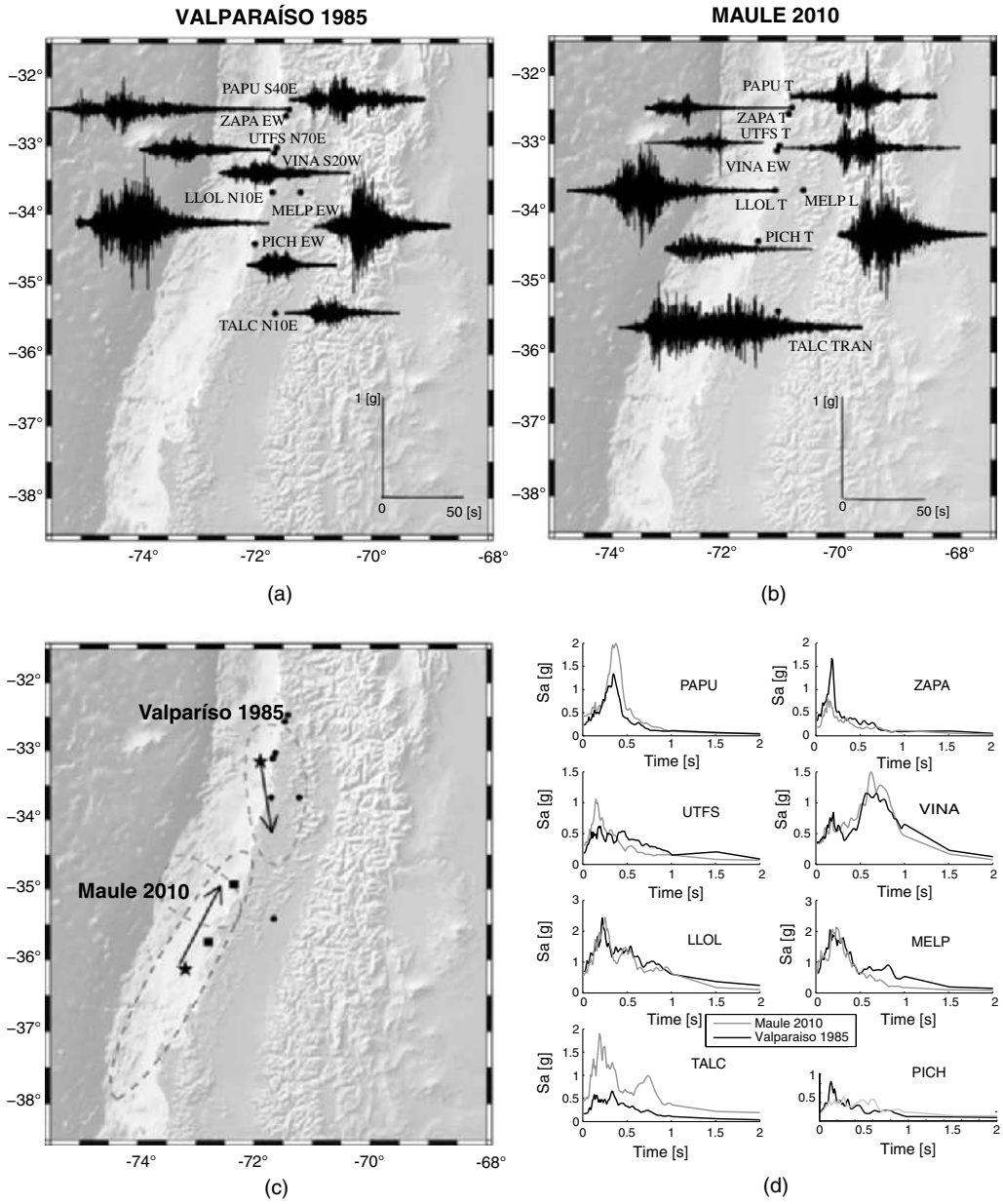

Figure 10. Strong motion records for the Valparaíso 1985 and Maule 2010 earthquakes. (a) Strong motion records of the 1985 Valparaíso earthquake at selected stations. (b) Strong motion recorded during the Maule 2010 at the same stations. (c) Schematic view of rupture propagation for the two earthquakes. Black stars are the epicenters of both events and black squares are the sites of the proposed asperities from the 2010 event (d) Comparison of response spectra at 5% damping for the strong motion records shown in parts (a) and (b).

important consequences for the excitation of tsunami waves by the Maule event (Fritz et al. 2011, Wu and Ho 2011). Further work on this particular point seems necessary.

The cGPS data are dominated by near-field surface and body waves that propagate in the crustal wave guide, while the short-period strong motion signals propagate like multiply scattered body waves. They show different sensitivity to the velocity model that is used to locate the asperities. We have to wait for the tomographic studies currently in preparation in order to improve the local velocity model.

The locations of asperities in the northern part of the Maule rupture may explain why the damage to rigid structures was concentrated in this zone, in contrast with the low damage observed south of the epicenter (Astroza et al. 2012).

The short-period rupture process observed during the Maule 2010 earthquake may not be only an attribute of the Maule megathrust earthquake. Frequency-dependent rupture behavior was also observed during the Tohoku, Japan, 2011 (M_w 9.0) earthquake by Koper et al. (2011), Meng et al. (2011), and Wang and Mori (2011) using back-propagation of high-frequency waves observed in far-field seismic arrays. Furthermore, moderate damage was observed during the Tohoku earthquake in comparison with shallow earthquakes (Kawase 2011), and recorded strong motion data were similar to that of previous M ~8.0 Japanese earthquakes like the 2003 Tokachi-oki earthquake (Si et al. 2011).

CONCLUSIONS

We studied the intermediate- and high-frequency radiation generated by the 2010 Maule earthquake using near-field high-rate GPS and strong motion records. Unfortunately these data are only available for the northern part of the rupture of the event, from Concepción (37.5°S) to the north. There seems to be no high-rate GPS instruments or usable strong motion data from the southern end of the rupture.

We inverted the ground velocities obtained by band-limited differentiation of the cGPS records in central Chile. Although the data are heavily dominated by the propagation of the rupture front, we could determine that a local asperity located roughly westward of the city of Constitución produced a significant part of the high frequency waves observed in local accelerograms. In all the stations situated north of Constitución, two big strong motion pulses are observed that we associated with the two asperities situated north of this city. Finally, a comparison with records from the 1985 Valparaíso earthquake shows that high-frequency emissions from that earthquake and from Maule were very similar in the northern stations. This similarity is striking in the envelopes of strong motion data and in the acceleration response spectra of accelerograms. Thus, it seems that the 2010 earthquake was huge at low frequencies, but the strong motion was very similar to that of a smaller event of magnitude 8. Similar observations have been reported for the recent 2011 Tohoku earthquake.

ACKNOWLEDGEMENTS

The authors would like to thank the Seismological National Service (SSN) and the National Network of Civil Department (RENADIC) of the University of Chile for making records of the 2010 Maule earthquake available to us. Sergio Ruiz and Jaime Campos have been partially funded by Millennium Nucleus Program “Montessus de Ballore—IERC,”

Mideplan, Chile, and Laboratoire International Associé (L.I.A) CNRS, Universidad de Chile. This work was supported by FONDECYT contract No. 1100429 in Chile and by ANR Risk, contract DEBATE ANR-08-RISK-001, in France.

REFERENCES

Astroza, M., Ruiz, S., and Astroza, R., 2012. Damage assessment and seismic intensity analysis of the 2010 (M_w 8.8) Maule earthquake, *Earthquake Spectra* **28**, this issue.

Boroschek, R., Contreras, V., Kwak, D. Y., and Stewart, J. P., 2012. Strong ground motion attributes of the 2010 Mw 8.8 Maule, Chile, earthquake, *Earthquake Spectra* **28**, this issue.

Bouchon, M., 1981. A simple method to calculate Green's functions for elastic layered media, *Bull. Seismol. Soc. Am.* **71**, 959–971.

Campos, J., Hatzfeld, D., Madariaga, R., Lopez, G., Kausel, E., Zollo, A., Barrientos, S., and Lyon-Caen, H., 2002. The 1835 seismic gap in South Central Chile, *Phys. Earth Planet. Int.* **132**, 177–195.

Comte, D., Eisenberg, A., Lorca, E., Pardo, M., Ponce, L., Saragoni, R., Singh, S. K., and Suarez, G., 1986. The 1985 central Chile earthquake: A repeat of previous great earthquakes in the region?, *Science* **233**, 449–453.

Coutant, O., 1990. *Programme de Simulation Numerique AXITRA*, Rapport LGIT, Univ. Joseph Fourier, Grenoble, France.

Delouis, B., Nocquet, J. M., and Vallée, M., 2010. Slip distribution of the February 27, 2010 M_w = 8.8 Maule earthquake, central Chile, from static and high-rate GPS, InSAR, and Broadband teleseismic data, *Geophysical Research Letters* **37**, L17305, doi:10.1029/2010GL043899.

Di Carli, S., François-Holden, C., Peyrat, S., and Madariaga, R., 2010. Dynamic inversion of the 2000 Tottori earthquake based on elliptical subfault approximations, *J. Geophys. Res.* **115**, B12328, doi:10.1029/2009JB006358.

Earthquake Engineering Research Institute (EERI), 1986. The Chile earthquake of March 3, 1985: Introduction, *Earthquake Spectra* **2**, 249–252.

Engdahl, E. R., and Villaseñor, A., 2002. Global seismicity: 1900–1999, in The International Handbook of Earthquake and Engineering Seismology, Part A (W. H. K. Lee, H. Kanamori, P. C. Jennings, and C. Kisslinger, editors), Academic Press, New York, 665–690.

Fritz, H. M., Petroff, C. M., Catalán, P. A., Cienfuegos, R., Winckler, P., Kalligeris, N., Weiss, R., Barrientos, S. E., Meneses, G., Valderas-Bermejo, C., Ebeling, C., Papadopoulus, A., Contreras, M., Almar, R., Dominguez, J. C., and Synolakis, C. E., 2011. Field survey of the 27 February 2010 Chile tsunami, *Pure Appl. Geophys*. **168**, 1989–2010, doi:10.1007/s00024-011-0283-5.

Heaton, T. H., 1990. Evidence for and implication of self-healing pulses of slip in earthquake rupture, *Phys. Earth Planet. Int.* **64**, 1–20.

Housner, G. W., 1963. An engineering report on the Chilean earthquakes of May 1960: Preface, *Bull. Seismol. Soc. Am*. **53**, 219–223.

Kanamori, H., and Stewart, G. S., 1978. Seismological aspects of the Guatemala earthquake of February 4, 1976, *J Geophys Res* **83**, 3427–3434.

Kawase, H., 2011. Strong motion characteristics and their damage impact to structures during the off Pacific coast of Tohoku earthquake of March 11, 2011: How extraordinary was this M9.0 earthquake?, in *Proceedings, 4th IASPEI/IAEE International Symposium*, Santa Barbara, EEUU.

Kiser, E., and Ishii, M., 2011. The 2010 M_w 8.8 Chile earthquake: Triggering on multiple segments and frequency dependent rupture behavior, *Geophys. Res. Lett.*, doi:10.1029/2011GL047140.

Koper, K., Hutko, A., Lay, T., Ammon, C., and Kanamori, H., 2011. Frequency-dependent rupture process of the 2011 M_w 9.0 Tohoku earthquake: Comparison of short-period *P* wave back projection images and broadband seismic rupture models, *Earth Planets Space* **63**, 599–602.

Lay, T., Ammon, C. J., Kanamori, H., Koper, K. D., Sufri, O., and Hutko, A. R., 2010. Teleseismic inversion for rupture process of the 27 February 2010 Chile (M_w 8.8) earthquake, *Geophys. Res. Lett*. **37**, L13301, doi:10.1029/2010GL043379.

Lorito, S., Romano, F., Atzori, F., Tong, X., Avallone, A., McCloskey, J., Cocco, M., Boshi, E., and Piatanesi, A., 2011. Limited overlap between the seismic gap and co-seismic slip of the great 2010 Chilean earthquake, *Nature Geoscience Letters*, doi:10.1038/NGEO1073.

Madariaga, R., Vigny, C., Métois, M., and Campos, J., 2010. Central Chile finally breaks, *Science* **328**, 181–182.

Meng, L., Inbal, A., and Ampuero, J. P., 2011. A window into the complexity of the dynamic rupture of the 2011 M_w 9 Tohoku-Oki earthquake, *Geophys. Res. Lett.* **38**, L00G07, doi:10.1029/2011GL048118.

Moreno, M., Melnick, D., Rosenau, M., Bolte, J., Klotz, J., Echtler, H., Baez, J., Bataille, K., Chen, J., Bevis, M., Hase, H., and Oncken, O., 2011. Heterogeneous plate locking in the south-central Chile subduction zone: Building up the next great earthquake, *Earth Planet Sci. Lett.* **305**, 413–424.

Pollitz, F. F., Brooks, B., Tong, X., Bevis, M. G., Foster, J. H., Bürgmann, R., Smalley, Jr., R., Vigny, C., Socquet, A., Ruegg, J.-C., Campos, J., Barrientos, S., Parra, H., Soto, J. C. B., Cimbaro, S., and Blanco, M., 2011. Coseismic slip distribution of the February 27, 2010 M_w 8.8 Maule, Chile earthquake. *Geophys. Res. Lett.* **38**, L09309, doi:10.1029/2011GL047065.

Pulido, N., Yagi, Y., Kumagai, H., and Nishimura, N., 2011. Rupture Process and coseismic deformations of the 27 February 2010 Maule earthquake, *Earth Planets Space* **63**, 1–4.

Ruiz, S., Kausel, E., Campos, J., Saragoni, G. R., and Madariaga, R., 2011. Identification of high frequency pulses from earthquake asperities along Chilean subduction zone using strong motion, *Pure and Applied Geophysics* **168**, 125–139.

Sambridge, M., 1999. Geophysical inversion with a neighbourhood algorithm—I. Searching a parameter space, *Geophys. J. Int.* **138**, 479–494.

Si, H., Kuyuk, H. S., Koketsu, K., and Miyake, H., 2011. Attenuation characteristic of peak ground motion during the 2011 Tohoku, Japan, earthquake, *Seismol. Res. Lett.* **82**, 460.

Servicio Sismológico (SSN), 2010. Servicio Sismológico, Universidad de Chile Departamento de Geofísica, available at http://www.sismologia.cl/seismo.html.

U.S. Geological Survey (USGS), 2010. *Preliminary Determination of Epicenter Bulletin*.

Tong, X., Sandwell, D., Luttrell, K., Brooks, B., Bevis, M., Shimada, M., Foster, J., Smalley, Jr., R., Parra, H., Báez Soto, J. C., Blanco, M., Kendrick, E., Genrich, J., and Caccamise, D. J., 2011. The 2010 Maule, Chile earthquake: Downdip rupture limit revealed by space geodesy, *Geophys. Res. Lett.*, doi:10.1029/2010GL045805.

Vallée, M., and Bouchon, M., 2004. Imaging coseismic rupture in far field by slip patches, *Geophys. J. Int.* **156**, 615–630.

Vigny, C., Socquet, A., Peyrat, S., Ruegg, J. C., Métois, M., Madariaga, R., Morvan, S., Lancieri, M., Lacassin, R., Campos, J., Carrizo, D., Bejar-Pizarro, M., Barrientos, S., and Armijo, R.,

SSN Team, LIA-MdB Team, and CAP Team, 2011. The 2010 (M_w 8.8) Maule megathrust earthquake of central Chile, monitored by GPS, *Science* **332**, 1417–1421.

Wang, D., and Mori, J., 2011. Frequency dependent energy radiation and fault coupling for the 2010 M_w 8.8 Maule, Chile, and 2011 M_w 9.0 Tohoku, Japan, earthquakes, *Geophys. Res. Lett.*, doi:10.1029/2011GL049652.

Wu, T. R., and Ho, T. C., 2011. High resolution tsunami inversion for 2010 Chile earthquake, *Nat. Hazards. Earth. Sci.* **11**, 3251–3261.

Yoffe, E., 1951. The moving Griffith crack, *Phil. Mag.* **42**, 739–750.

(Received 17 March 2011; accepted 14 March 2012)